Optics & Laser Technology 50 (2013) 55–64

Contents lists available at SciVerse ScienceDirect

Optics & Laser Technology

journal homepage: www.elsevier.com/locate/optlastec

Review

Design of ultra compact all-optical XOR, XNOR, NAND and OR gates using photonic crystal multi-mode interference waveguides

Weijia Liu [a,b], Daquan Yang [a,b], Guansheng Shen [a,b], Huiping Tian [a,b], Yuefeng Ji [a,b,*]

[a] State Key Laboratory of Information Photonics and Optical Communications, Beijing 100876, China
[b] School of Information and Communication Engineering, Beijing University of Posts and Telecommunications, Beijing 100876, China

ARTICLE INFO

Article history:
Received 17 September 2012
Received in revised form
13 December 2012
Accepted 28 December 2012

Keywords:
All-optical logic gate
Multi-mode interference
Binary-phase-shift-keyed signals

ABSTRACT

We propose ultra compact all-optical XOR, XNOR, NAND and OR gates based on photonic crystal multi-mode interference waveguides for binary-phase-shift-keyed signals. The logic gates have been simulated and analyzed by finite difference time domain method. The extinction ratio between the ON state and the OFF state for XOR, XNOR, NAND and OR gates are more than 28.6 dB, 28.6 dB, 25 dB and 26.6 dB in the whole C-band, respectively. The proposed structure can achieve logical function when the radius of all rods is fabricated with relaxed error tolerance within −10% to 30% from designed parameters. The device possesses ultra compact size with approximately 6.9 μm × 6.7 μm. The proposed logic gates may potentially be used as key components in all-optical information networks for processing binary-phase-shift-keyed signals.

Contents

1. Introduction

All-optical signal processing techniques are expected to be the main supporting techniques in future all-optical information networks [1,2]. As key components in all-optical networks, all-optical logic gates would achieve various networking functions [3] such as addressing, and header recognition, etc.

On the other hand, binary-phase-shift-keyed (BPSK) format has been studied extensively owing to its better optical signal noise ratio (OSNR) and nonlinearity tolerance than the on-off-keyed (OOK) format, especially in ultra-long-haul submarine systems [4–7]. Therefore, it is truly significant to design the device with logic functions for BPSK signals.

However, during the past few decades, most all-optical logic gates were achieved for OOK signals [8–10]. The all-optical logics

* Corresponding author at: Beijing University of Posts and Telecommunications, P.O. Box 90, Xitucheng Road, Beijing 100876, China. Tel./fax: +86 10 6228 2153.
E-mail address: jyf@bupt.edu.cn (Y. Ji).

0030-3992/$ - see front matter Crown Copyright © 2013 Published by Elsevier Ltd. All rights reserved.
http://dx.doi.org/10.1016/j.optlastec.2012.12.030

for BPSK signals have been reported very little except the optical logic gates based on multi-mode interference waveguides reported in [11]. In order to design the logic gate with simple structure, ultra compact size and without additional control light, we adopt photonic crystals (PCs). PCs offer great promise in designing key ultra compact devices in all-optical integrated circuits with significant reduction in the size and power consumption. The size of PCs all-optical logic gates can be reduced to the order of wavelength. Many all-optical logic gates based on photonic crystal have been reported [12–19], and these photonic crystal logic gates have potential to be key component in future integration circuit. It is highly significant to design the devices that possess lower power consumption, more compact size and higher fabrication error tolerance for BPSK signals and large-scale integrated system.

Multimode interference waveguides are attracted by some scholars [20–23], especially for photonic crystal multimode interference waveguides are widely applied in the design of all-optical devices, including all-optical logic gate [19], terahertz photonic crystal switch [23], wavelength de-multiplexing [24,25], and polarization beam splitter [26,27], due to their simple structure, low loss and large optical bandwidth.

In this paper, we propose all-optical XOR, XNOR, NAND and OR functions based on photonic crystal multimode interference waveguides. For our designed logic gates, the logical value of the input is determined only by the phase information, and the logical value of the output is determined only by the amplitude information. Finite difference time domain (FDTD) method has been used for numerical simulations, and the FDTD method can be performed by the simulation software of Rsoft. The extinction ratio between the ON state and the OFF state for XOR, XNOR, NAND and OR gates are no less than 28.6 dB, 28.6 dB, 25 dB and 26.6 dB in the whole C-band (1530 nm–1565 nm), respectively. In addition, we discuss the fabrication tolerance of the logic gate. The proposed device can achieve logic functions and keep good performance when the radius of all rods is fabricated with error tolerance within −10% to 30% from designed parameters.

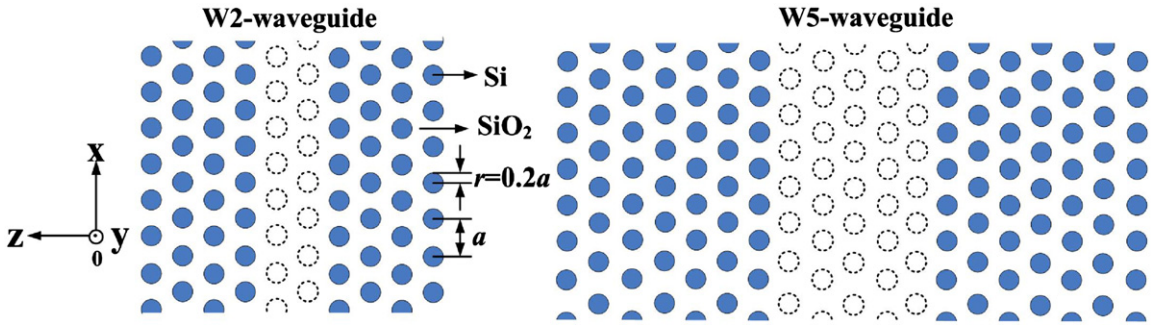

Fig. 1. Schematic of W2-waveguide and W5-waveguide.

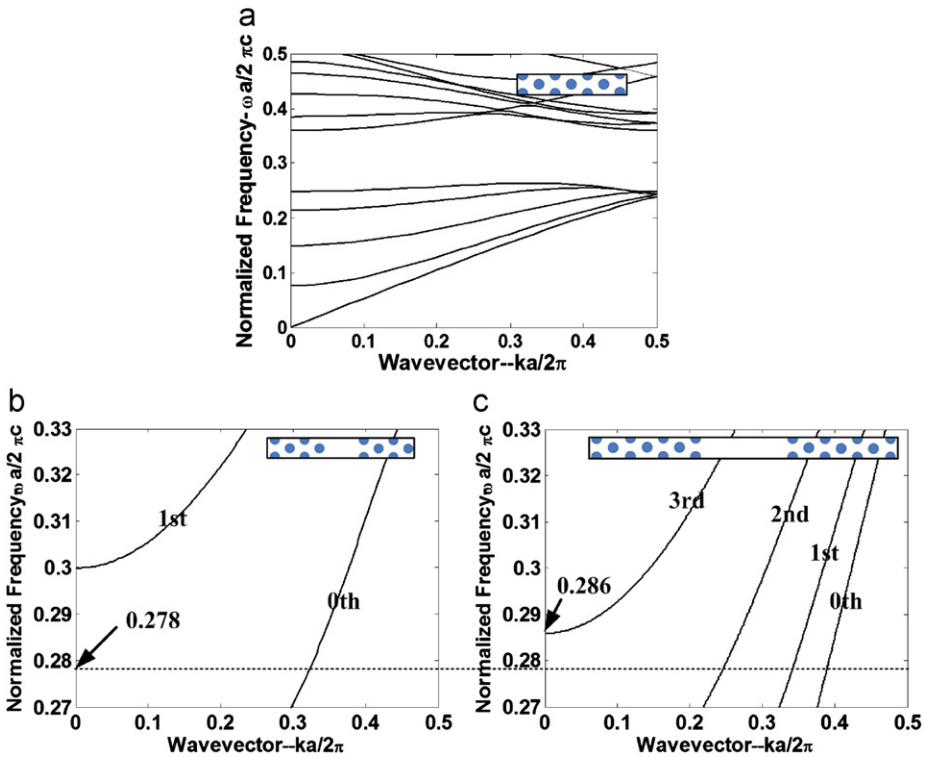

Fig. 2. (a) Dispersion curves for the prefect photonic crystal and the computational super-cell (inset). (b) Dispersion curves for the W2-waveguide and the computational super-cell (inset). (c) Dispersion curves for the W5-waveguide and the computational super-cell (inset).

2. Theory analysis

2.1. Guided mode property

We will design the all-optical logic gates based on two kinds of photonic crystal waveguides that W2 and W5-waveguide as shown in Fig. 1, where W*n* stands for a PC waveguide with *n* rows of dielectric rods removed along the Γ-K direction of the crystal (the removed rods from waveguides are marked as dashed circle as shown in Fig. 1). Here, we consider two dimensional photonic crystal waveguide structures composed of triangular lattice Si rods in SiO_2 background. The refractive index of the Si rods is 3.48 and their radius r is 0.2a, where a is the lattice constant of photonic crystal. The refractive index of the background-SiO_2 is 1.45.

The dispersion curves of perfect photonic crystal, W2-waveguide and W5-waveguide are calculated by plane wave expansion (PWE) method, respectively. The band gap of the perfect photonic crystal exists in the frequency ranges of 0.2622∼0.3596 (a/λ) with TM polarization, as shown in Fig. 2(a). The dispersion curves of W2-waveguide and W5-waveguide are illustrated in Fig. 2(b) and (c), respectively, and the insets are the super-cells used for calculation. From Fig. 2(b) and (c), we can see that for the two waveguides, W2-waveguide holds one mode between frequency of 0.286(a/λ) and the top of band gap, therefore ensure single-mode propagation in this frequency range. The W5-waveguide holds three modes between frequency of 0.286(a/λ) and the top of band gap therefore ensure multi-mode propagation in this frequency range.

If we use four guided modes of W5 waveguide to produce self-imaging effect, the operation frequency should be located in the frequency scope between 0.286 and 0.3. But this operation frequency scope is very small and is not suitable for designing the optical devices, and therefore we consider choosing three guided modes of W5 waveguide to produce self-imaging effect, and the operation frequency scope should be located in the scope between 0.286 and the top of band gap. And next, we simulate the mode field to find the optimal operation frequency which can let optical signal propagate well. And the simulation results can be seen in Figs. 3 and 4. Figs. 3 and 4 show the mode filed in frequency 0.275, 0.278, and 0.282 (a/λ) for W2 and W5 waveguide, and it can be seen that the mode field is strongest in 0.278 (a/λ). Therefore we choose the frequency of 0.278 (a/λ) to serve as operation frequency of optical device.

2.2. Self-imaging theory

The mode propagation analysis (MPA) method is very useful to describe the self-imaging phenomena in multimode waveguide [26]. It is assumed that the input wave is well confined to the guiding region not to excite the radiation modes. So the total field $\psi(x, z)$ in the multi-mode waveguide at a distance x can be expressed as a sum of all guided modes [26]:

$$\psi(x,\ z) = \sum_{n=0}^{p-1} c_n \phi_n(z) \exp\left[j(\beta_0 - \beta_n)\right) x] \tag{1}$$

where $\varphi_n(z)$ is the modal field distribution, c_n is the field excitation coefficient, p is the number of modes, and the subscript n denotes the order of modes ($n=0, 1, 2, \ldots, p-1$). $\exp[j(\beta_0-\beta_n)x]$ is mode phase factor, where β_0 and β_n are the propagation constants of the fundamental mode and the nth mode. The field excitation coefficient c_n can be estimated using overlap integrals based on the field-orthogonality relation as

$$c_n = \frac{\int \psi(x,\ z)\phi_n(z)dz}{\int \phi_n^2(z)dz} \tag{2}$$

The profile of $\psi(x, z)$ and the types of images formed are determined by the modal excitation coefficient c_n and by the properties of the mode phase factor exp $[j(\beta_0-\beta_n)x]$. The shortest coupling length between the fundamental mode and the nth mode is defined as [23]:

$$L_c = \frac{\pi}{\beta_0 - \beta_n} \tag{3}$$

We choose the frequency of 0.278(a/λ) to study. The parameters about these modes at 0.278(a/λ), including propagation constant, the symmetry property of modal field patterns and the

Table 1
Parameters about the modes of W5-waveguide for TM waves at 0.278 (a/λ).

Frequency (a/λ)	Mode number-n	Parity	Propagation constant-$\beta(2\pi/a)$	$Lc=\pi/(\beta_0-\beta_n)$
0.278	Zero order-0	even	0.3896	—
	First order-1	odd	0.3425	10.5a
	Second order-2	even	0.247	3.5a

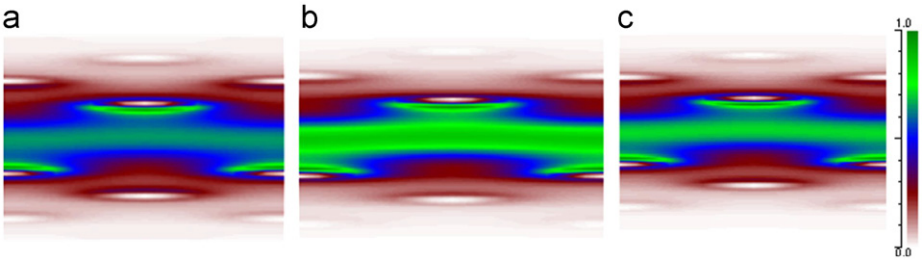

Fig. 3. Mode field in frequency (a) 0.275(a/λ), (b) 0.278(a/λ), (c) 0.282(a/λ) for W2 waveguide.

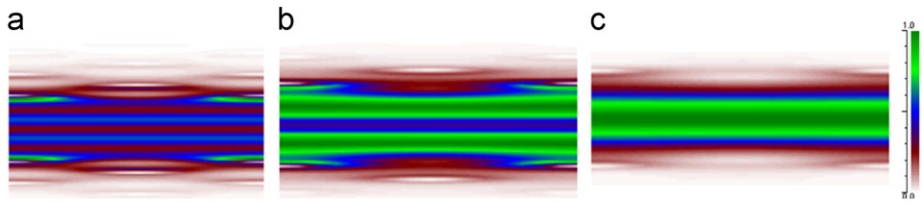

Fig. 4. Mode field in frequency (a) 0.275(a/λ), (b) 0.278(a/λ), (c) 0.282(a/λ) for W5 waveguide.

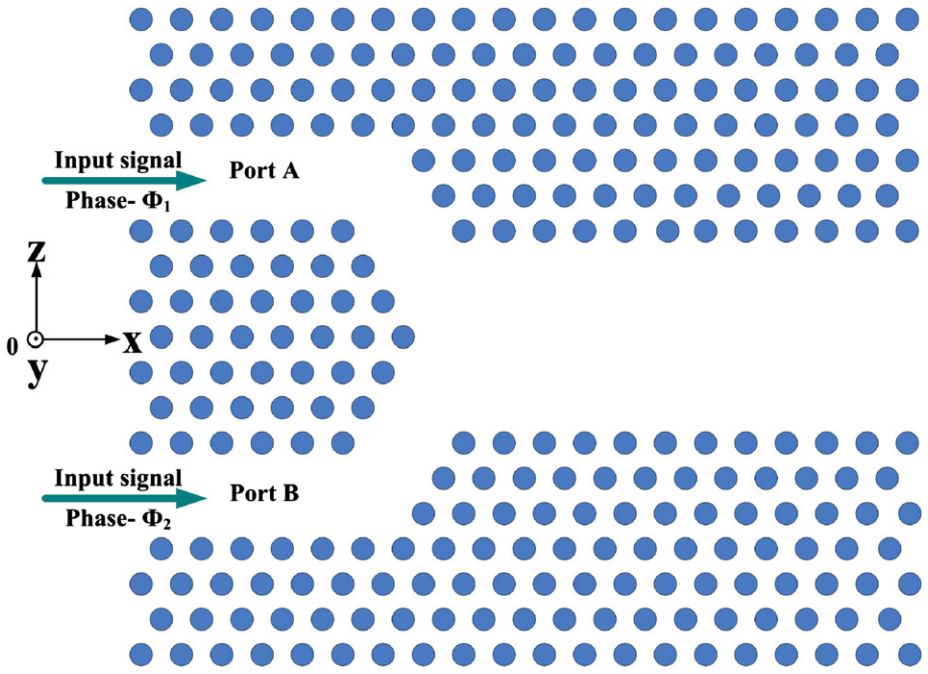

Fig. 5. Open-ended W5-waveguide with two input ports.

coupling length L_c, are listed in Table 1. According to (3), L_c between zero order mode and first order mode is 10.5a, and L_c between zero order mode and second order mode is 3.5a at 0.278(a/λ).

2.3. Logic model design

In order to design the appropriate length for multimode interference (MMI) region to achieve logical function, we firstly study on the open-ended W5-waveguide [26] as shown in Fig. 5. If the two input light with the same phase are launched into the two input ports at the same time, the components along z direction of the two inputs light will cancel out, and the components along x direction of the two inputs light will be superimposed. This case is equivalent to that one input light is launched vertically into the W5-waveguide at $z=0$ along the x direction, and then single image and double image will appear alternatively [27]. If the input light with the different phase is launched at the same time, in those positions where zero order mode couples with first order mode and second order mode, some coupling components of the two inputs will canceled out because of opposite phase and other coupling components of the two inputs will be superimposed because of same phase. In order to achieve logical function, we need to find the appropriate position that the superimposed components will emerge at only one side of the MMI region as much as possible, then the output ports will be laid at this position to get maximum output light power.

To design the appropriate length of W5-waveguide and verify the above-mentioned analyses, we observe the steady-state field distributions in an open-ended W5 waveguide, as shown in Fig. 6, by using the 2D FDTD method. The phase difference (Φ_1–Φ_2) is assumed to be 90°, −90°, 0° and 180°, where Φ_1 and Φ_2 are the phases of two inputs light on port A and port B, respectively. It is assumed that two input light signals have the same intensity, wavelength and polarization.

From Fig. 6, we can see that there are some expected phenomena occurred in the position where the length of MMI is 3.5a. When input light with $\Phi1=0^\circ$ on port A and input light with $\Phi2=-90^\circ$ on port B are launched into W2-waveguide at the same time, light superimposes on one side of the W5-waveguide. When input light with $\Phi1=0^\circ$ on port A and input light with $\Phi2=90^\circ$ on port B are launched into W2-waveguide at the same time, light superimposes on other side of the MMI region. When input light with $\Phi1=0^\circ$on port A and input light with $\Phi2=0^\circ$ on port B are launched into W2-waveguide at the same time, single image and double image of input light appear alternatively in MMI region. When input light with $\Phi1=180^\circ$on port A and input light with $\Phi2=0^\circ$ on port B are launched into W2-waveguide at the same time, two input light propagate along two sides of MMI region.

Through prior self-imaging theoretical analysis, we know that the shortest coupling length L_c between zero order mode and second order mode is 3.5a at 0.278(a/λ),which is close to 4a. Therefore, we infer that L_c between zero order mode and second order mode is the appropriate length of W5-waveguide. Therefore, we choose 4a as the length of the W5-waveguide; the basic logic model is designed as show in Fig. 7. Where port C serves as logic output port; port A and port B serve as two input ports.

3. Optimization and analysis for the logic model

3.1. Optimization for the logic model

We optimize the logic model shown in Fig. 7 for three aspects of extinction ratio, conversion efficiency and transmission ratio. The structure of MMI mainly influences the performance of logic gate, especially the rods around the MMI. We firstly study the impact of rods-A (shown in Fig. 7) on the performance of logic gate. We shift the rods-A to observe the change of the transmission ratio and extinction ratio, while input light with phase $\Phi_1=0^\circ$on port A and input light with phase $\Phi_2=-90^\circ$ and 90° on port B. Two input light signals have the same intensity, wavelength and polarization. The direction of shifting rods-A is signed as Fig. 7 (lined out as red arrow) and the distance of shifting is defined as d. Then we calculate the transmission ratio and extinction ratio of the logic model with various d, and the results are shown in Figs. 8 and 9, respectively. The transmission

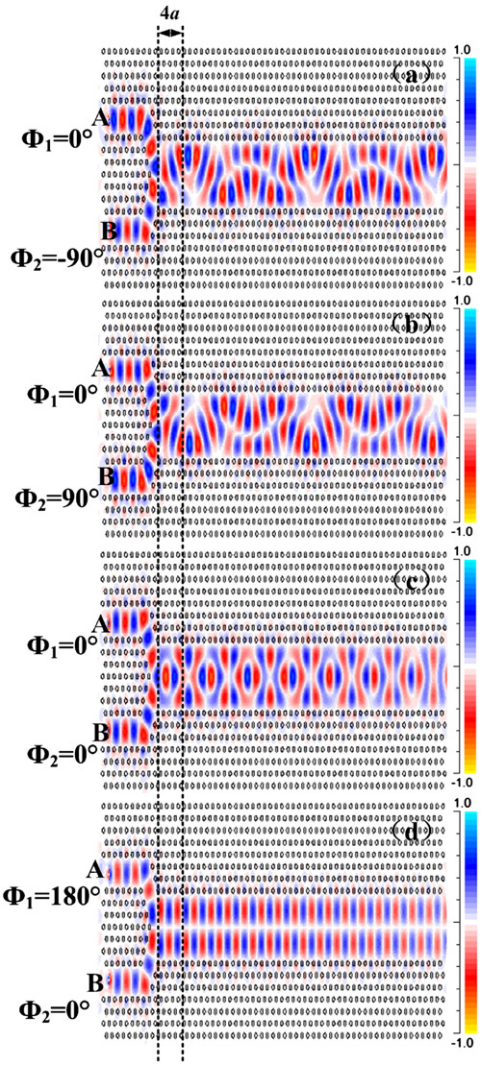

Fig. 6. Field distributions at the 1550 nm for open-ended W5-waveguide.

is defined as

$$TR = \frac{P_C}{P_A + P_B} \times 100\% \tag{4}$$

where P_C is the power of the logic output port C and P_A+P_B is the total input power. The extinction ratio is defined as [11]:

$$\mathrm{ER} = 10 \log_{10} \frac{\mathrm{P_1}}{\mathrm{P_0}} \tag{5}$$

where P_1 is power of logic 1 obtained on output port C and P_0 is power of logic 0 obtained on output port C, respectively. For the logic output port, logic 1 is achieved when logic output port have maximum output power, and logic 0 is achieved when logic output port have minimum output power.

From Fig. 8, we can see that only the concave transmission peak (lined out as dashed elliptical) move to low frequency when increasing the shifting-distance d. Comparing to the peak when $d=0$, the peak when d is bigger than 0 are all located in the frequency that is lower than the case of $d=0$. Only when $d=0.4a$, the peak move to the high frequency, but this high frequency is also lower than the frequency of the peak when $d=0$. Therefore, from the whole moving tendency, the peak moves to lower frequency. Therefore, the shifting of rods-A can increase the bandwidth of normalized transmission of not less than 80%, and the bandwidth is widest when d is $0.5a$. The shifting of rods-A also can increase the operating bandwidth of the ON to OFF logic-level extinction ratio of not less than 15 dB as shown in Fig. 9, and the bandwidth is widest when d is $0.5a$. The shifting-distance d is set as $0.5a$. According to $a=\lambda \times f$, where a is lattice constant, λ is the work wavelength of the logic gate, and f is the operation frequency of logic gate. We can adjust the logic model to operate at the whole C-band by setting lattice-constant $a=1550 \times 0.278\ \mathrm{nm} \approx 430\ \mathrm{nm}$.

Next we study the impact of rods-B on the performance of the logic gate. In our proposed logic gate, W5-waveguide serves as MMI. We modify radius of the first row rods-B (shown in Fig. 5) of W5-waveguide to observe the change of the extinction radio, while input light with phase $\Phi_1=0^\circ$on port A and input light with phase $\Phi_2=-90^\circ$ and 90° on port B. The results are shown in Fig. 10. From Fig. 10, we can see that when the radius R is $0.17a$, the ER is more than 28.6 dB with frequency scope from 1522 nm to 1566 nm. The ER of the case of $R=0.17a$ is higher than other cases, and have wider frequency bandwidth than other cases when ER is 28.6 dB. Through optimization above, we propose logic gate model as shown in Fig. 7, where the shifting distance of rods-A is $d=0.5a$ and the radius of rods-B is $R=0.17a$.

3.2. Performance analysis

We analyze the extinction ratio, conversion efficiency and transmission ratio of all-optical logic gate model shown as in Fig. 7. The extinction ratio is shown as Fig. 10, and we can see that the extinction ratio is more than 28.6 dB in the whole C-band (1530–1565 nm).

We change the phase Φ_1 of input light on port A from -180° to 180° while phase Φ_2 of input light on port B is 90°. The conversion efficiency η is defined as [11]:

$$\eta = \frac{P_C}{P_{max}} \times 100\% \tag{6}$$

where P_C is the power of logic output port C, and P_{max} is the maximum output power. The conversion efficiency spectra are shown in Fig. 11. We can see that the change case of conversion efficiency with phase Φ_1 when phase Φ_2 is fixed.

Fig. 12 shows the wavelength dependence of the transmission in the whole C-band for the logic model. From Fig. 12, we can see that, the transmission of logic model is over 93% in the whole C-band.

4. Examples of the logic gate with XOR, XNOR, NAND and OR functions

4.1. Definition of logic value for BPSK signals and logical behavior analysis

The proposed logic gate can operate two-channel BPSK signals and can achieve different logic functions for different combinations of BPSK signals. Next, we will discuss XOR, XNOR, NAND and OR logic functions as examples to illustrate the logic behaviors of the proposed logic gate.

For each logical function, it is achieved by inputting two kinds of BPSK signals (BPSK1 on input port A and BPSK2 on input port B) and corresponding logical definition of logic 1 and 0 is illustrated in Table 2. It can be seen from Table 2; the logic gate will process these two signals for XOR calculation when BPSK1 with logic 1 and 0 defined by phase $0^\circ$and 180°respectively and BPSK2 with logic 1 and 0 defined by phase $90^\circ$and -90°respectively; the logic gate will process these two signals for XNOR calculation when BPSK1 with logic 1 and 0 defined by phase $0^\circ$and 180°respectively and BPSK2 with logic 1 and 0 defined by phase $-90^\circ$and

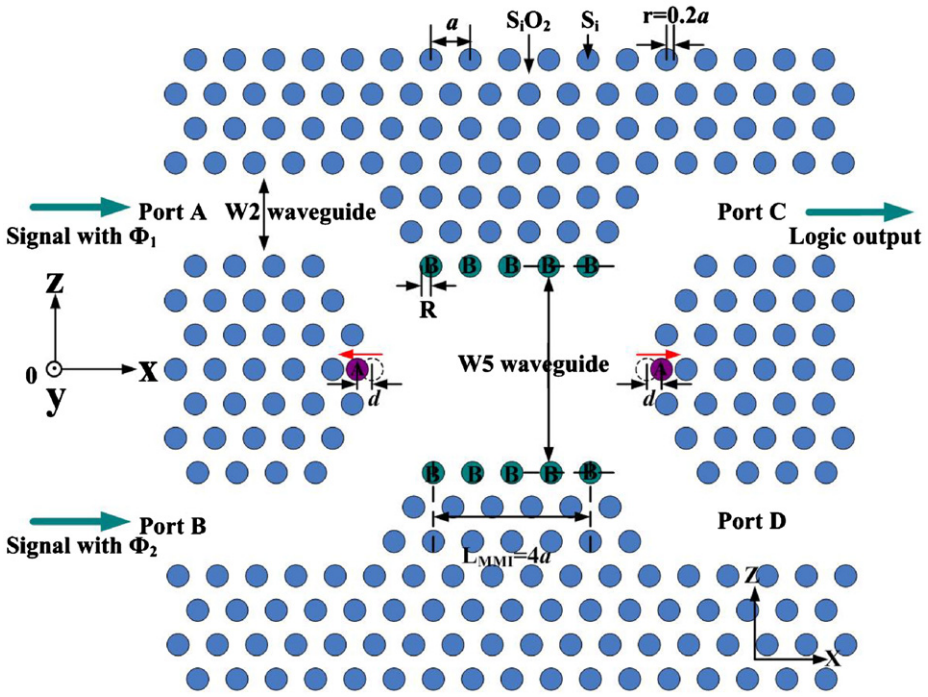

Fig. 7. Structure of logic model with XOR, XNOR, NAND and OR functions. (For interpretation of the references to color in this figure, the reader is referred to the web version of this article.)

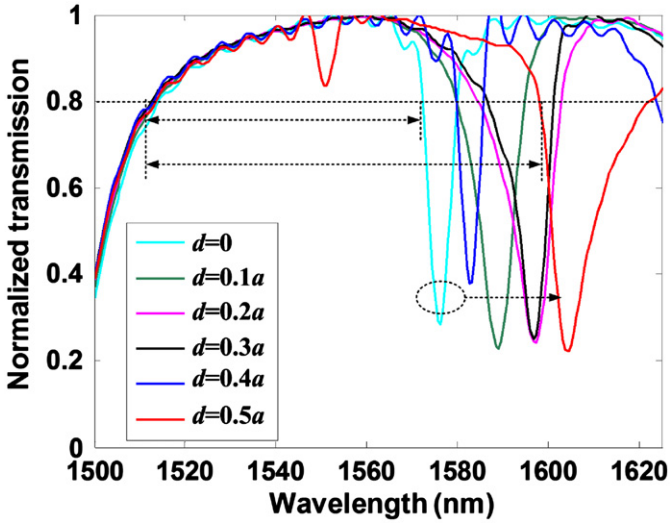

Fig. 8. Transmission ratio as a function of normalized frequency with various *d*.

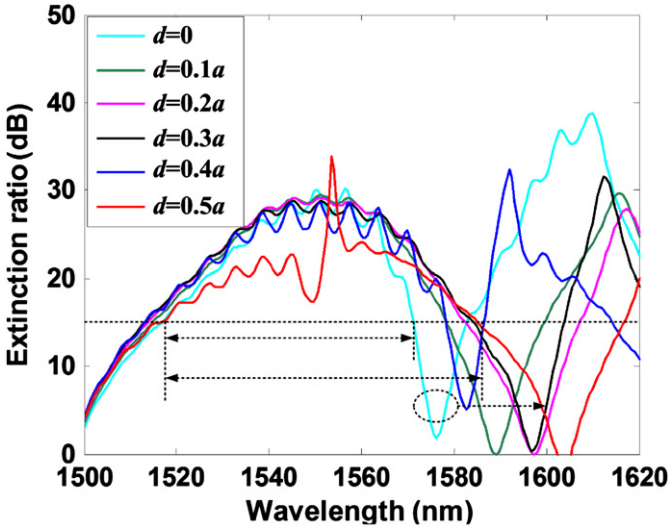

Fig. 9. Extinction ratio as a function of normalized frequency with various *d*.

90°respectively; the logic gate will process these two signals for NAND calculation when BPSK1 with logic 1 and 0 defined by phase −90°and 90°respectively and BPSK2 with logic 1 and 0 defined by phase 0°and 90°respectively; the logic gate will process these two signals for OR calculation when BPSK1 with logic 1 and 0 defined by phase 180°and 0°respectively and BPSK2 with logic 1 and 0 defined by phase 180°and 90°respectively. In order to illustrate the principle of processing BPSK signals better, we give the corresponding schemas of logic gate with XOR, XNOR, NAND and OR logical functions for different BPSK signals respectively, as shown in Fig. 13.

Then, we simulate proposed logic gate and measure its logical output for different kinds of combinations of the inputs which can achieve XOR, XNOR, NAND and OR functions according to Table 3. The field distributions of logic gate at the whole-C band with XOR, XNOR, NAND and OR functions are shown in Fig. 14. The behavior of logic gate with XOR, XNOR, NAND and OR functions for simulation is in accordance with Table 3. Therefore, this proposed all-optical logic gate can function as XOR, XNOR, NAND and OR gates for different input BPSK signals.

4.2. Extinction property of logic gate

We analyze the extinction property of this logic gate for XOR, XNOR, NAND and OR functions, respectively. The extinction rate of logic output port C is calculated as (7) which is defined as [11]:

$$ER = 10\log_{10}\frac{P_y}{P_x} \tag{7}$$

where P_y and P_x is power of logic 1 and logic 0 obtained on output port C, respectively. Subscript *y* and *x* represents operation step 1,

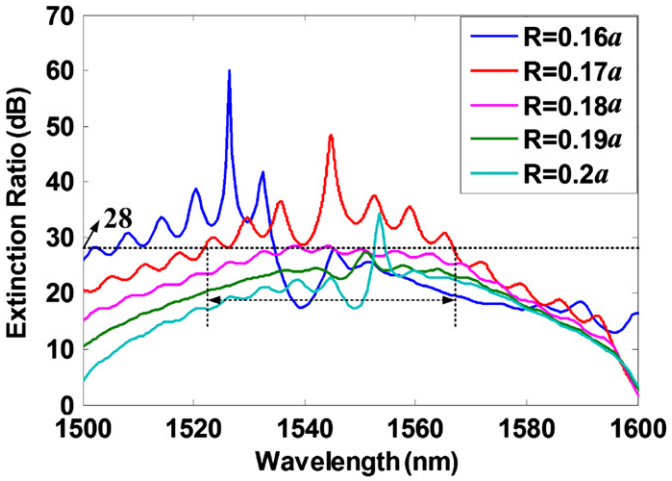

Fig. 10. Extinction ratio as a function of normalized frequency with different *R*.

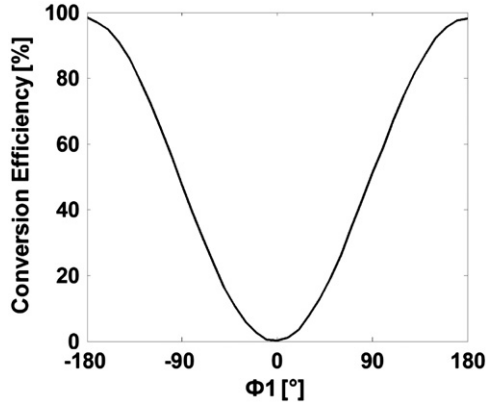

Fig. 11. (a) Conversion Efficiency of logic model, when phase-Φ_2 of input light on port B is 90°.

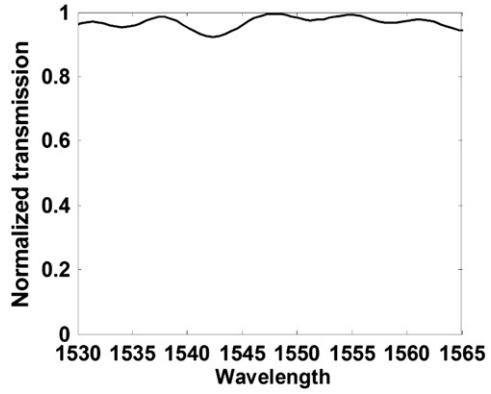

Fig. 12. Normalized transmission of logic model, where *a* is 430 nm.

Table 2
The definition of logic value of BPSK signals on input ports (A and B).

Logic functions	Port-A BPSK1 Logic value		Port-B BPSK2 Logic value	
	1 Phase	0 Phase	1 Phase	0 Phase
XOR	0°	180°	90°	−90°
XNOR	0°	180°	−90°	90°
NAND	−90°	90°	0°	90°
OR	180°	0°	180°	90°

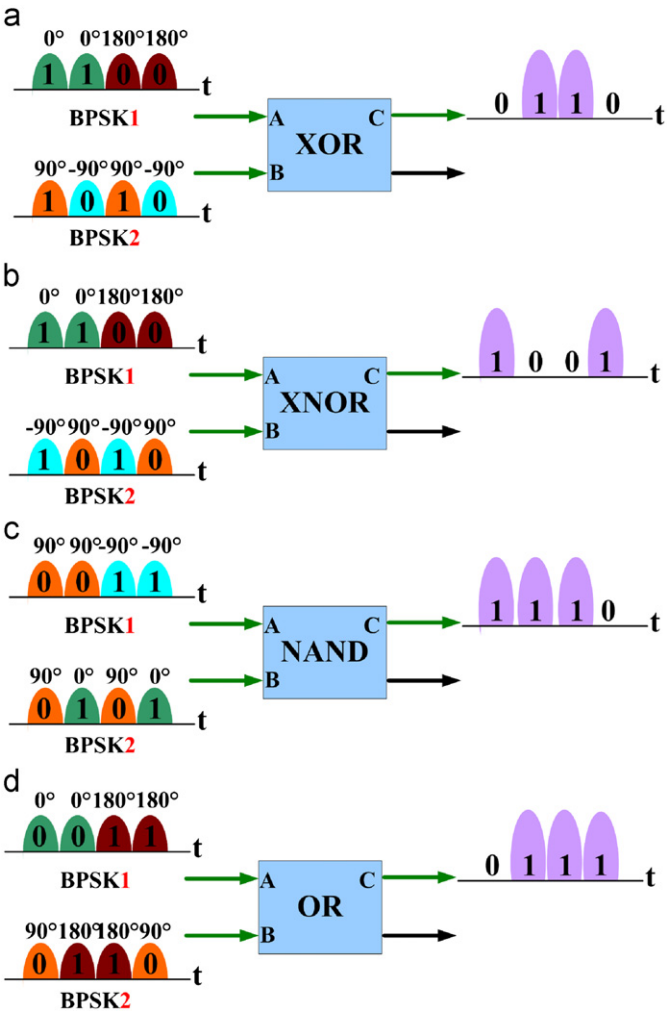

Fig. 13. (a), (b), (c) and (d) are schemas of logic gate with XOR, XNOR, NAND and OR logical functions for different BPSK signals, respectively.

2, 3 and 4 shown as Table 3, respectively. The extinction rate of logic output port C for XOR, XNOR, NAND and OR functions is shown in Fig. 15(a), (b), (c) and (d), respectively. As shown in Fig. 15(a) and (b), the extinction ratio of logic gate with XOR and XNOR functions almost exceeds 28.6 dB on the whole C-band (1530 nm–1565 nm). The extinction ratio of our proposed XOR structure may exhibit a better performance than the XOR structures in [11,17,19], the minimum extinction ratio of XOR structure in [11] is 21.5 dB in the whole C-band, the extinction ratio of XOR structure in [17] is between 17 dB and 20.1 dB, and the

Table 3
Truth table for the XOR, XNOR, NAND and OR gates.

Operation steps	Logic input		Logic output on Port-C			
	Port-A	Port-B	XOR	XNOR	NAND	OR
1	1	1	0	1	0	1
2	1	0	1	0	1	1
3	0	1	1	0	1	1
4	0	0	0	1	1	0

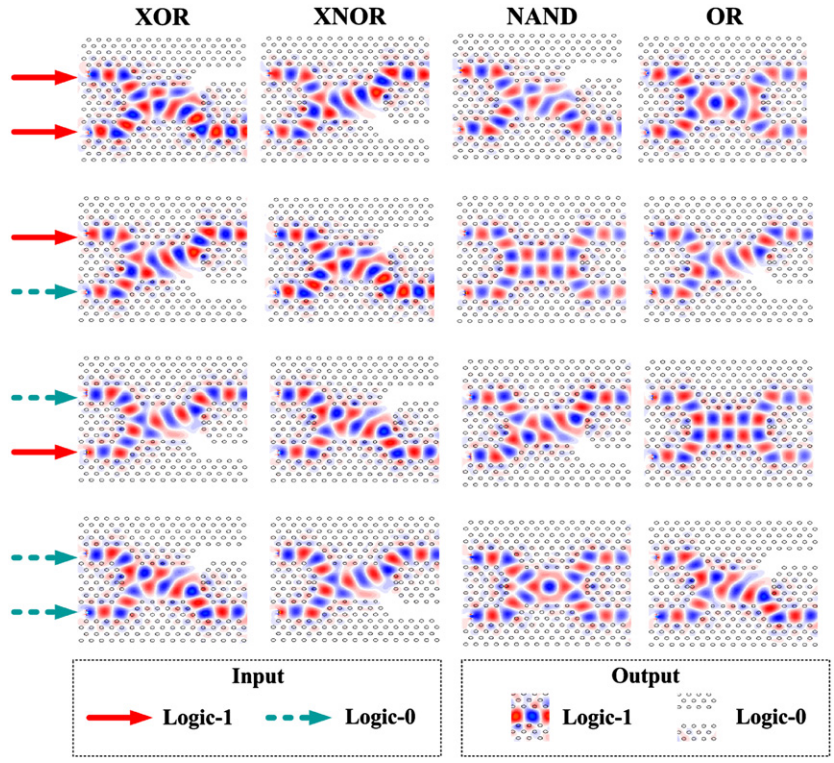

Fig. 14. Field distributions to show the performance of the proposed all-optical logic gate with XOR, XNOR, NAND and OR functions for different BPSK signals, respectively.

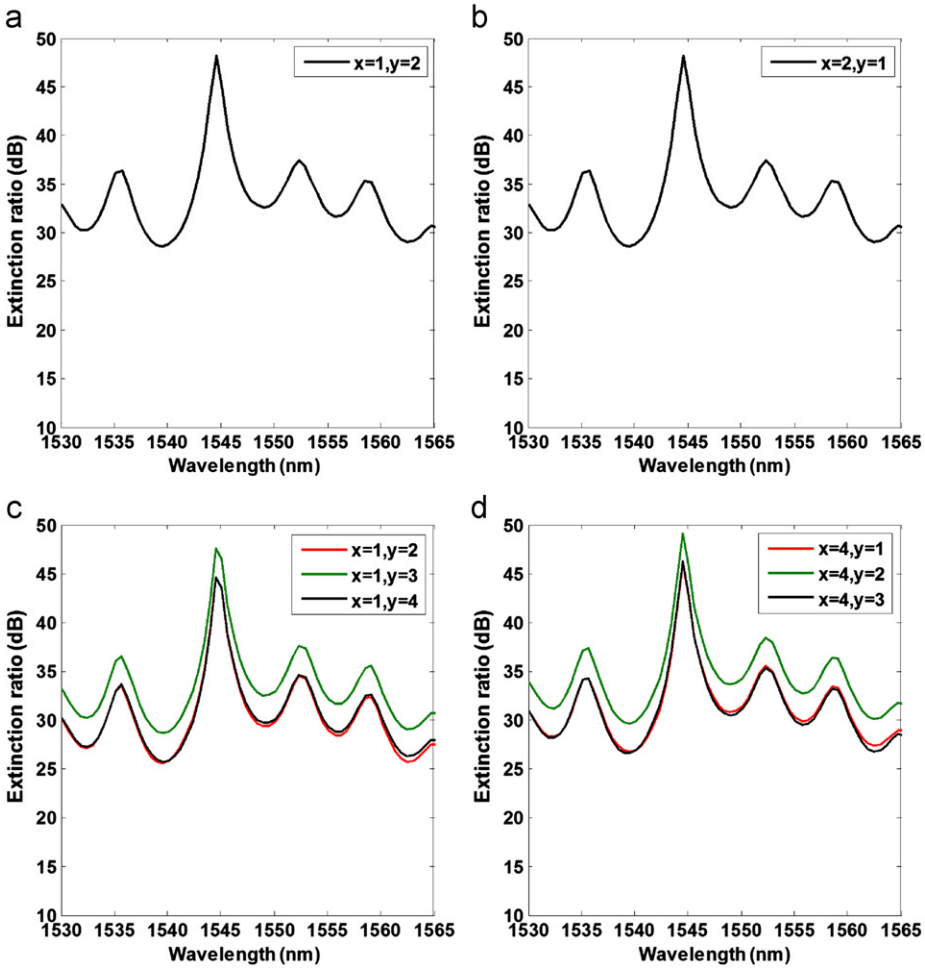

Fig. 15. (a), (b), (c) and (d) are extinction ratio of the logic gate with XOR, XNOR, NAND and OR functions, respectively.

minimum extinction ratio of XOR structure in [19] is 6.79 dB in the whole C-band. As shown in Fig. 15(c) and (d), we can see the extinction ratio of logic gate with NAND and OR functions almost exceed 25 dB and 26.6 dB on the whole C-band, respectively. The extinction ratio of our proposed logic gate with OR function may exhibit a better performance than the OR structure in [11], and the minimum extinction ratio of OR structure in [11] is 22.3 dB in the whole C-band.

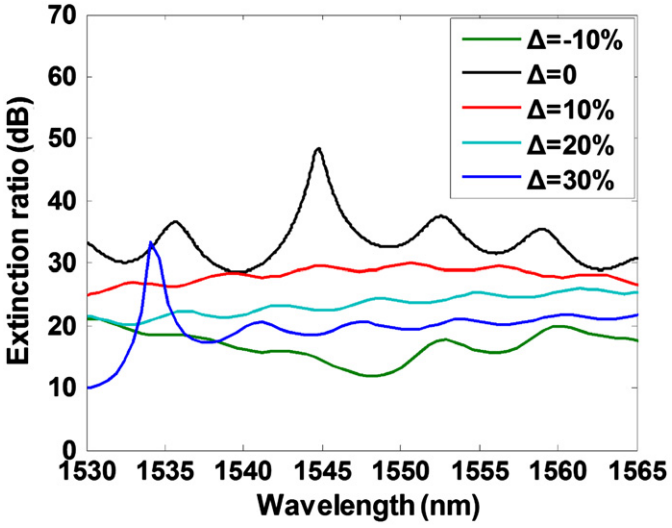

Fig. 16. Fabrication error tolerance of XOR model.

5. Analyses of fabrication tolerance

In order to analyze the practical applications of the above-mentioned logic models, we will discuss the fabrication error tolerance of logic model-XOR gate. We assume that all the rods radius in the logic models with Δ% error from theoretical designed parameters, and the fabrication tolerance Δ can be express as follows:

$$R_{error} = R_{theory} \times 1 + \Delta \tag{8}$$

where R_{error} is the radius of each rod that has error comparing to theory design value, R_{theory} is theory design value of the radius of each rod, and Δ is the error proportion and is named error tolerance. Then we have calculated the spectrum of the extinction ratio when all the rods are -10%, 10%, 20% and 30% larger than theoretical designed parameters, as shown in Fig. 16. From Fig. 17, we can see that, for $\Delta = -10$%, 10%, 20% and 30%, the ON to OFF logic level extinction ratio in the whole C-band is 10 dB, 25 dB,

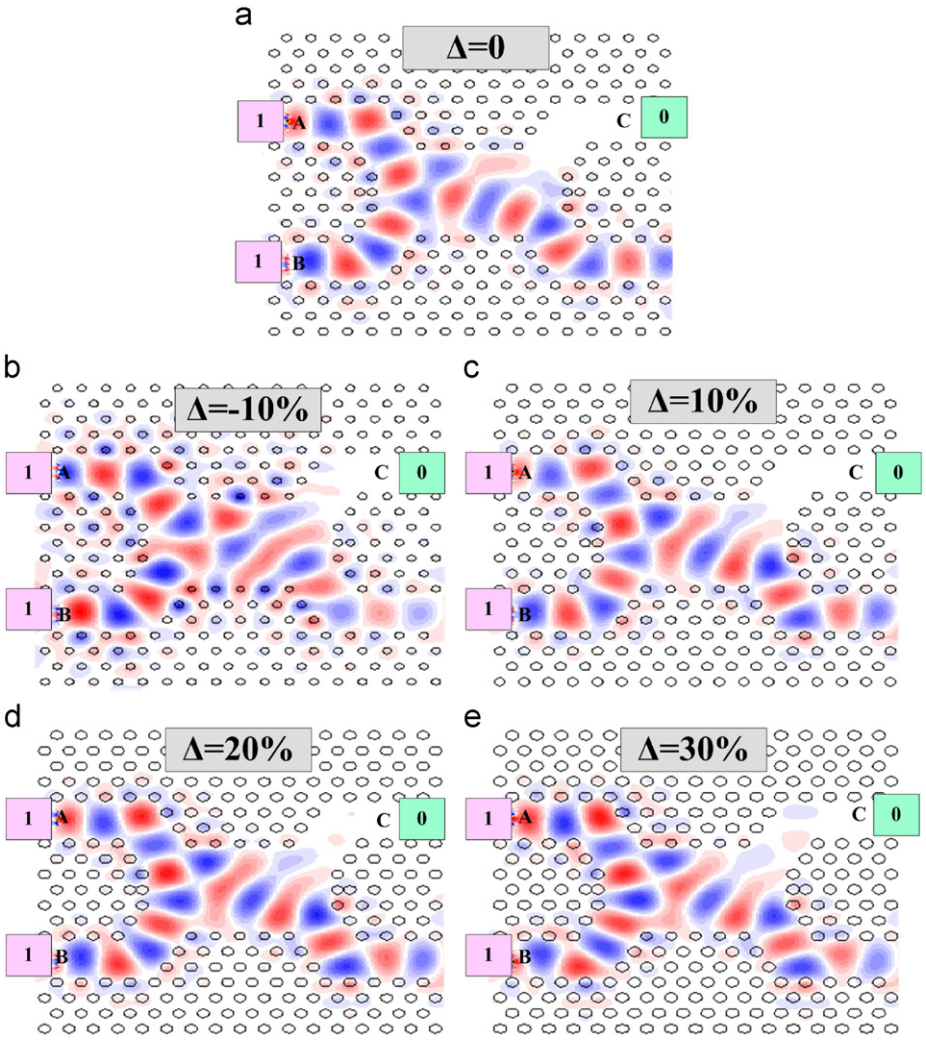

Fig. 17. Field distributions of the logic model with XOR function (a)–(e) at $\lambda = 1550$ nm with Δ% error. On Port A, $\Phi_1 = 0^\circ$ and 180° represent logic 1 and logic 0, respectively. On Port B, $\Phi_1 = 90^\circ$ and -90° represent logic 1 and logic 0, respectively.

Table 4
Operating bandwidth $\Delta\lambda$ of the ON and OFF logic-level extinction ratio not less than one value with Δ% error.

	ER (dB)	$\Delta\lambda$ (nm)
$\Delta=0$	≥ 28.6	35
$\Delta=-10\%$	≥ 10	35
$\Delta=10\%$	≥ 25	35
$\Delta=20\%$	≥ 20	35
$\Delta=30\%$	≥ 10	35

20 dB and 10 dB, respectively. We summarize the analytical results of operating bandwidth $\Delta\lambda$ of the ON and OFF logic-level extinction ratio more than one value when the model has Δ error in Table 4. The field distributions of XOR gate at $\lambda=1550$ nm with Δ% error are illustrated in Fig. 17. The fabrication error tolerance of our proposed logic model may exhibit a better performance than logic structure in [19]. The rods radius of the XOR logic [19] needs to be controlled with not more than 5% fabrication error through simulation analysis, and rods radius of the logic model in this paper can be controlled within -10% to 30% fabrication error with well performance.

6. Conclusion

We propose photonic crystal all-optical XOR, XNOR, NAND, and OR logic gates based on multi-mode interference waveguide. The device operations for the TM wave have been simulated and analyzed by the FDTD method. The device possesses ultracompact size with approximately 6.9 μm × 6.7 μm. We analyze the performance of proposed logic structure for extinction ratio, conversion efficiency, transmission ratio and fabricate tolerance. The ON and OFF logic-level extinction ratio for XOR, XNOR, NAND and OR gates are more than 28.6 dB, 28.6 dB, 25 dB and 26.6 dB in the whole C-band, respectively. The conversion efficiency is no less than 98%. The transmission ratio is no less than 93% in the whole C-band. And we analyze the fabrication tolerance of the XOR logic model, when all rods radius are larger than criteria parameters from -10% to 30%. For $\Delta=-10\%$, 10%, 20% and 30%, the ON to OFF logic level extinction ratio in the whole C-band is 10 dB, 25 dB, 20 dB and 10 dB, respectively. The device is potentially important for future all-optical information integrated networks.

Acknowledgments

This research was supported in part by National 973 Program (No. 2012CB315705), National 863 Program (No. 2012AA011301, 2011AA010306), NSFC (No. 61171103), PR China.

References

[1] Ji YueFeng, Ren DanPing, Li Hui, Liu XueJun, Wang ZhengZhong. Analysis and experimentation of key technologies in service-oriented optical internet. Science China 2011;54(2):215–26.
[2] Xu Jing, Zhang Xinliang, Zhang Yin, Dong Jianji, Liu Deming, Huang Dexiu. Reconfigurable all-optical logic gates for multi-input differential phase-shift keying signals: design and experiments. Journal of Lightwave Technology 2009;27(23):5268–75.
[3] Ramos F, Kehayas E, Martinez JM, Clavero R, Marti J, Stampoulidis L, et al. IST-LASAGNE: towards all-optical label swapping employing optical logic gates and optical flip-flops. Journal of Lightwave Technology 2005;23(10): 2993–3011.
[4] Yan Meng, Tao Zhenning, Zhang Huijian. Adaptive blind equalization for coherent optical BPSK system ECOC; 2010.
[5] Gnauck AH, Chandrasekhar S, Leuthold J, Stulz L. Demonstration of 42.7 Gb/s DPSK receiver with 45 photons/bit sensitivity. IEEE Photonics Technology Letters 2003;15(1):99–101.
[6] Gnauck AH, Raybon G, Chandrasekhar S, Leuthold J, Doerr C, Stulz L, et al. 25 40 Gb/s copolarized DPSK transmission over 12 100-km NZDF with 50-GHz channel spacing. IEEE Photonics Technology Letters 2003;15(3):467–9.
[7] Mizuochi T, Ishida K, Kobayashi T, Abe J, Kinjo K, Motoshima K, et al. A comparative study of DPSK and OOK WDM transmission over transoceanic distances and their performance degradations due to nonlinear phase noise. Journal of Lightwave Technology 2003;21(9):1933–43.
[8] Wu Yaw-Dong, Shih Tien-Tsorng. New all-optical logic gates based on the local nonlinear Mach-Zehnder interferometer. Optics Express 2008;16(1): 248–57.
[9] Xu Qianfan, Lipson Michal. All-optical logic based on silicon micro-ring resonators. Optics Express 2007;15(3):924–9.
[10] Zhang Xinliang, Wang Ying, Sun Junqiang, Liu Deming, Huang Dexiu. All-optical AND gate at 10 Gbit/s based on cascaded single-port-coupled SOAs. Optics Express 2004;12(3):361–6.
[11] Ishizaka Yuhei, Kawaguchi Yuki, Koshiba Masanori. Design of optical XOR, XNOR, NAND, and OR logic gates based on multi-mode interference waveguides for binary-phase-shift-keyed signal. Journal of Lightwave Technology 2011;29(18):2836–46.
[12] Liu Qiang, Ouyang Zhengbiao, Wu Chih Jung, Liu Chung Ping, Wang C. All-optical half adder based on cross structures in two-dimensional photonic crystals. Optics Express 2008;16(23):18992–9000.
[13] Andalib Parisa, Granpayeh Nosrat. All-optical ultracompact photonic crystal AND gate based on nonlinear ring resonators. Journal of the Optical Society of America B 2009;26(1).
[14] Liu Bin, Tian Huiping, Lu Hui, Ji Yuefeng. Nonlinearity-controllable all-optical logic gates based on broadband defect mode. Optical Applications 2010;XL(3).
[15] Zhu Zhi-Hong, Ye Wei-Min, Ji Jia-Rong, Yuan Xiao-Dong, Zen Chun. High-contrast light-by-light switching and AND gate based on nonlinear photonic crystals. Optics Express 2006;14(5):1783–8.
[16] Kabilan AP, Susan Christina X, Elizabeth Caroline P. Photonic crystal based all optical OR and XO logic gates. International Conference on Computing Communication and Networking Technologies, 2010, pp. 1–4.
[17] Zhang Yuanliang, Zhang Yao, Li Baojun. Optical switches and logic gates based on self-collimated beams in two-dimensional photonic crystals. Optics Express 2007;15(15):9287–92.
[18] Husko C, Vo TD, Corcoran B, Li J, Krauss TF, Eggleton BJ. Ultracompact all-optical XOR logic gate in a slow-light silicon photonic crystal waveguide. Optics Express 2011;19(21):20681–90.
[19] Ishizaka Yuhei, Kawaguchi Yuki, Saitoh Kunimasa, Koshiba Masanori. Design of ultra compact all-optical XOR and AND logic gates with low power consumption. Optics Communications 2011;284:3528–33.
[20] Zang Z, Mukai K, Navaretti P, Duelk M, Velez C, Hamamoto K. Thermal resistance reduction in high power superluminescent diodes by using active multi-mode interferometer,. Applied Physics Letters 2012;100:031108.
[21] Zang Z, Minato T, Navaretti P, Hinokuma Y, Duelk M, Velez C, et al. High power(>110 mW) superluminescent diodes using active multi-mode interferometer. IEEE Photonics Technology Letters 2010;22(10):721–3.
[22] Zang Z, Mukai K, Navaretti P, Duelk M, Velez C, Hamamoto K. High power and stable high coupling efficiency (66%) superluminescent light emitting diodes by using active multi-mode interferometer. IEICE Transactions on Electronics 2011;E94-C(5):862–4.
[23] Li Zhangjian, Zhang Yao, Li Baojun. Terahertz photonic crystal switch in silicon based on self-imaging principle. Optics Express 2006;14(9):3887–92.
[24] Kim Hyun-Jun, Park Insu, Beom-Hoan O, Park Se-Geun, Lee El-Hang, Lee Seung-Gol. Self-imaging phenomena in multi-mode photonic crystal line-defect waveguides: application to wavelength de-multiplexing. Optics Express 2004;12(23):5625–33.
[25] Zhu Qile, Li Baojun. Photonic crystal waveguide-based Mach Zehnder demultiplexer. Applied Optics 2006;45(35).
[26] Lu Ming-Feng, Liao Shan-Mei, Huang Yang-Tung. Ultracompact photonic crystal polarization beam splitter based on multimode interference. Applied Optics 2010;49(4).
[27] Zhang Yao, Li Zhangjian, Li Baojun. Multimode interference effect and self-imaging principle in two-dimensional silicon photonic crystal waveguides for terahertz waves. Optics Express 2006;14(7):2679–89.